Accepted Manuscript

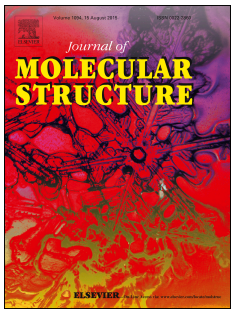

New fluorescent heterocyclic systems from imidazo[1,2-*a*]pyridine: Design, synthesis, spectral studies and quantum-chemical investigations

Mehdi Pordel, Hamed Chegini, Shirin Ramezani, Mohammadreza Daee

PII: S0022-2860(16)30915-2

DOI: 10.1016/j.molstruc.2016.08.085

Reference: MOLSTR 22911

To appear in: *Journal of Molecular Structure*

Received Date: 2 May 2016

Revised Date: 29 August 2016

Accepted Date: 31 August 2016

Please cite this article as: M. Pordel, H. Chegini, S. Ramezani, M. Daee, New fluorescent heterocyclic systems from imidazo[1,2-*a*]pyridine: Design, synthesis, spectral studies and quantum-chemical investigations, *Journal of Molecular Structure* (2016), doi: 10.1016/j.molstruc.2016.08.085.

Graphical Abstract

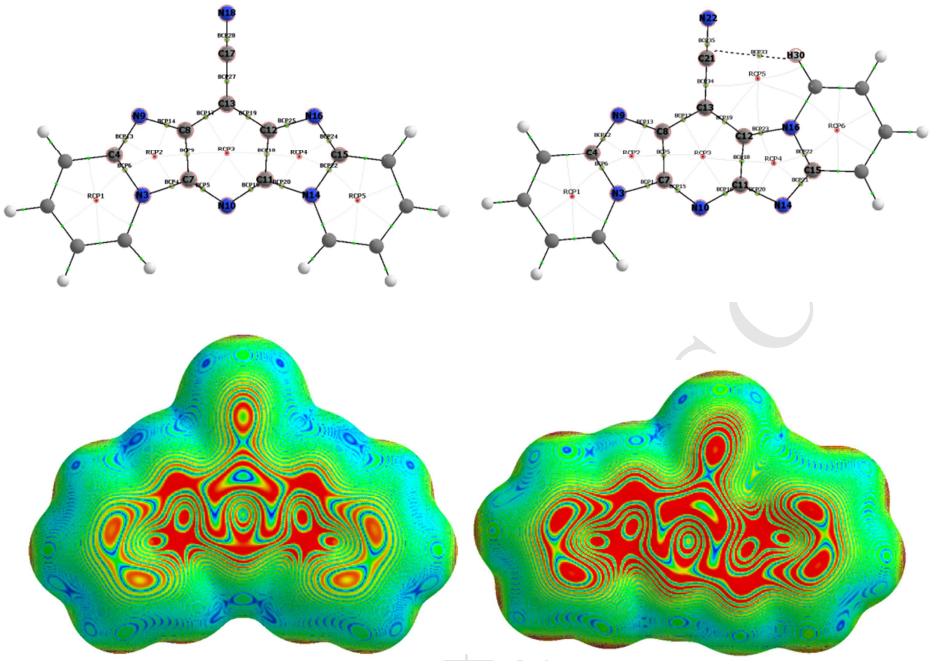

New fluorescent heterocyclic systems from imidazo[1,2-*a*]pyridine: Design, synthesis, spectral studies and quantum-chemical investigations

Mehdi Pordel *, Hamed Chegini, Shirin Ramezani and Mohammadreza Daee

Department of Chemistry, Mashhad Branch, Islamic Azad University, Mashhad, Iran

**Corresponding author. Tel.: +98 0513 8414182; fax: +98 0513 8424020. E-mail: mehdipordel58@mshdiau.ac.ir*

Abstract- Two new fluorescent heterocyclic systems dipyrido[1',2':1,2]imidazo[4,5-*b*:4,5-*e*]pyridine-13-carbonitrile and pyrido[1',2':1,2]imidazo[4,5-*b*]pyrido[2',1':2,3]imidazo[4,5-*e*]pyridine-13-carbonitrile were synthesized by one-pot reaction of imidazo[1,2-*a*]pyridine with 2-(imidazo[1,2-*a*]pyridin-3-yl)acetonitrile and 2-(imidazo[1,2-*a*]pyridin-2-yl)acetonitrile, respectively, in MeOH/KOH solution *via* the nucleophilic substitution of hydrogen in high yields. Spectral and analytical data have confirmed the structures of the synthesized dyes. The optical and solvatochromic properties of the compounds were investigated and the results showed that they exhibited interesting photophysical properties. Density functional theory (DFT) calculations of fluorescent dyes were performed to provide the optimized geometries and relevant frontier orbitals by using the B3LYP hybrid functional and the 6-311 ++ G(d,p) basis set. Calculated electronic absorption spectra were also obtained by time-dependent density functional theory (TD-DFT) method. In addition, electron density *iso*-surface map, intra- and intermolecular interactions of these fluorescent heterocyclic systems were evaluated by AIM (Atoms in Molecules) analysis.

Keywords: Imidazo[1,2-*a*]pyridine; Fluorescence; Emission and absorption spectra; Density functional theory; AIM analysis.

1. Introduction

The heterocycles constitute the largest group and most varied family of organic compounds and are becoming ever more important in all aspects of pure and applied chemistry. Heterocyclic compounds count among their number many natural products, such as hormones, vitamins, alkaloids, antibiotics, as well as pharmaceuticals, herbicides, dyes, and other products of technical importance (corrosion inhibitors, antiaging drugs, sensitizers, stabilizing agents, etc.). Among various heterocycles, imidazo[1,2-*a*]pyridines are an important class of heterocyclic compounds. They are found in many biologically active compounds such as antiviral [1], anticancer [2], anxiolytic [3], antimalarial [4], hypnotic [5], antiprotozoal [6] and anti-inflammatory [7] agents, which has rendered this ring system quite an attractive target. This heterocycle continues to be a very popular scaffold for the development of new bioactive molecules, which is maybe due to its simple preparation together with the success of some drugs possessing this skeleton. The best example continues to be Sanofi-Synthe´labo zolpidem (Stilnox®, Ambien®, Myslee®), a blockbuster for the treatment of sleeping disorders. Recently, imidazo[1,2-*a*]pyridine moieties became of interest as dye [8,9] and fluorescent compounds [8–10]. Furthermore, the analytical properties of some imidazo[1,2-*a*]pyridine derivatives demonstrate they can use as an acid–base indicator. The results show these compounds are superior to well-known indicators such as Quinaldine Red, Malachite Green, and Methyl Green in pH range 2–2.8 [11].

Taking these facts into consideration, in the present study, we have synthesized two new heterocyclic systems dipyrido[1',2':1,2]imidazo[4,5-*b*:4,5-*e*]pyridine-13-carbonitrile and pyrido[1',2':1,2]imidazo[4,5-*b*]pyrido[2',1':2,3]imidazo[4,5-*e*]pyridine-13-carbonitrile with interesting fluorescence properties. Density functional theory calculations (DFT) of fluorescent dyes were performed to provide the optimized geometries and relevant frontier orbitals. Furthermore, calculated electronic absorption spectra of the new fluorophores were obtained by TD-DFT method. Electron density *iso*-surface map, intra- and intermolecular interactions in these fluorophores were also studied by AIM analysis.

2. Experimental

2.1. Materials

Methanol, N,N-dimethylformamide (DMF), chloroform, 1,4-dioxane, acetonitrile (MeCN), cyclohexane, 2-bromo-1,1-dimethoxyethane, 1,3-dichloroacetone and 2-amino-pyridine were purchased from Merck. Potassium hydroxide was purchased from Sigma-Aldrich. All solvents were dried according to standard procedures. Compounds **1** and **2a,b** were synthesized as in literature [12–14].

2.2. Equipment

Absorption and fluorescence spectra were recorded on a Varian 50-bio UV–visible spectrophotometer and a Varian Cary Eclipse spectrofluorophotometer. UV–vis and fluorescence scans were recorded from 200 to 1000 nm. Melting points were measured on an Electrothermaltype-9100 melting-point apparatus. The IR (as KBr discs) spectra were obtained on a Tensor 27 spectrometer and only noteworthy absorptions are listed. The ^{13}C NMR (100 MHz) and the ^{1}H NMR (400 MHz) spectra were recorded on a Bruker Avance DRX-400 spectrometer in $CDCl_3$. Chemical shifts are reported in parts per million downfield from TMS as the internal standard; coupling constant *J* is given in hertz. The mass spectra were recorded on a Varian Mat, CH-7 at 70 eV. Elemental analysis was performed on a Thermo Finnigan Flash EA microanalyzer. All measurements were carried out at room temperature.

2.3. Computational methods

DFT calculations were performed with the Gaussian 98 software package [15] by using the B3LYP hybrid functional [16] and the 6-311++G(d,p) basis set. Firstly, geometry of the compounds **3** and **4** was fully optimized in the chloroform solution. The optimized geometry was confirmed to have no imaginary frequency. Then, their optimized geometry was used for frequency calculations.

Here, one of self-consistent reaction field methods, the sophisticated Polarized Continuum Model (PCM) [17] has been used for investigation of the solvent effects. The PCM calculations have been performed in the chloroform solution and the zero-point corrections were considered

to obtain energies. Based on the optimized geometries and using time-dependent density functional theory (TD-DFT) [18–20] methods, the electronic spectra of the compounds **3** and **4** were predicted.

*2.3. General procedure for the synthesis of **3** and **4**.*

3-Nitroimidazo[1,2-*a*]pyridine **1** (3.26 g, 20 mmol) and **2a,b** (25 mmol) were added with stirring to a solution of KOH (20 g, 357 mmol) in MeOH (80 mL). The mixture was stirred at rt for 24 h. After concentration at reduced pressure, the precipitate was collected by filtration, washed with water, following with cold EtOH and acetone respectively, and then air dried to give **3** and **4**. More purification was achieved by recrystallization from suitable solvent such as MeOH or EtOH.

Dipyrido[1',2':1,2]imidazo[4,5-*b*:4,5-*e*]pyridine-13-carbonitrile (3). Compound **3** was obtained as shiny yellow needles (EtOH), (69%), m.p.: 339–341 °C; IR (KBr disk): CN 2243 cm^{-1}; ^{1}H NMR: δ 7.21 (td, 1 H, J_1 = 6.8 Hz, J_2 = 1.9 Hz, Ar H); 7.24 (td, 1 H, J_1 = 6.7 Hz, J_2 = 2.1 Hz, Ar H); 7.83 (td, 1 H, J_1 = 6.6 Hz, J_2 = 2.2 Hz, Ar H); 7.90 (td, 1 H, J_1 = 6.9 Hz, J_2 = 2.4 Hz, Ar H); 7.95–8.04 (m, 2 H, Ar H); 9.21 (d, 1 H, J = 6.7 Hz, Ar H); 9.43 (d, 1 H, J = 6.8 Hz, Ar H) ppm; ^{13}C NMR (100 MHz): δ 97.3, 112.3, 119.4, 120.8, 121.9, 122.3, 125.4, 127.9, 129.6, 136.7, 139.5, 141.6, 146.1, 148.5, 154.7, 156.9 ppm; MS (EI, 70 eV), *m*/*z* (I_{rel} (%)): 284 $[M]^+$ (3); Found: C, 67.49; H, 2.82; N, 29.43. $C_{16}H_8N_6$ (284.3) Calculated (%): C, 67.60; H, 2.84; N, 29.56.

Pyrido[1',2':1,2]imidazo[4,5-*b*]pyrido[2',1':2,3]imidazo[4,5-*e*]pyridine-13-carbonitrile (4). Compound **4** was obtained as shiny yellow needles (MeOH), (75%), m.p.: 355–357 °C; IR (KBr disk): CN 2240 cm^{-1}; ^{1}H NMR: δ 7.35 (td, 2 H, J_1 = 6.8 Hz, J_2 = 1.8 Hz, Ar H); 7.86 (td, 2 H, J_1 = 7.1 Hz, J_2 = 2.1 Hz, Ar H); 8.05 (d, 2 H, J = 7.1 Hz, Ar H); 9.25 (d, 2 H, J = 6.8 Hz, Ar H) ppm; ^{13}C NMR (100 MHz): 1091.8, 117.3, 121.2, 122.3, 131.4, 137.9, 141.5, 144.2, 156.6 ppm; MS (EI, 70 eV), *m*/*z* (I_{rel} (%)): 284 $[M]^+$ (5); Found: C, 67.45; H, 2.81; N, 29.77. $C_{16}H_8N_6$ (284.3) Calculated (%): C, 67.60; H, 2.84; N, 29.56.

3. Results and Discussion

*3.1. Synthesis and structures of the new compounds **3** and **4***

As depicted in Scheme 1, the precursor of 3-nitroimidazo[1,2-*a*]pyridine **1** was obtained in two steps from the reaction of 2-aminopyridine with 2-bromo-1,1-dimethoxyethane. Nitration in H_2SO_4 and HNO_3 was accomplished by adopting a literature method [12]. Other precursor 2-(imidazo[1,2-*a*]pyridin-3-yl)acetonitrile **2a** was prepared by the reaction of imidazo[1,2-*a*]pyridine with Mannich reagent, MeI and KCN, respectively, in good yield [13]. The new heterocyclic systems dipyrido[1',2':1,2]imidazo[4,5-*b*:4,5-*e*]pyridine-13-carbonit **3** was synthesized *via* the nucleophilic substitution of hydrogen [21] of 3-nitroimidazo[1,2-*a*]pyridine **1** with 2-(imidazo[1,2-*a*]pyridin-3-yl)acetonitrile **2a** in basic MeOH solution and following with subsequent cyclization and dehydration at room temperature in high yield (Scheme 1). A tentative mechanism to explain the formation of compound **3** is shown in Scheme 2 [8,22].

<**Scheme 1**>

<**Scheme 2**>

Other new heterocyclic system pyrido[1',2':1,2]imidazo[4,5-*b*]pyrido[2',1':2,3]imidazo[4,5-*e*]pyridine-13-carbonitrile **4** was obtained in a similar mechanism. Nucleophilic substitution of hydrogen of 3-nitroimidazo[1,2-*a*]pyridine **1** with 2-(imidazo[1,2-*a*]pyridin-2-yl)acetonitrile **2b** which was readily obtained from the reaction of 2-(chloromethyl)*H*-imidazo[1,2-*a*]pyridine with KCN in H_2O under reflux using a literature method [14], led to the formation of new fluorophore **4** in excellent yield (Scheme 3). The work-up procedure was very simple, performed by filtration of the precipitated product after the mixture was concentrated at reduced pressure. Washing the precipitated product with suitable solvents (water and then acetone) gives practically pure compound **4**.

<**Scheme 3**>

The structural assignments of compounds **3** and **4** were based on the analytical and spectral data. For example, in the ^{1}H NMR spectrum of compound **4** revealed two triplet of doublet signals at δ_H 7.35 ppm and 7.86 ppm and two doublet peaks at δ_H 8.05 ppm and 9.25 ppm assignable to eight protons of aromatic rings. Moreover, the FT-IR spectrum of **4** in KBr showed an absorption band at 2240 cm^{-1} corresponding to cyanide group. Furthermore, the mass spectrum of this product shows the molecular ion m/z 284 (M^+), confirming its presumed structure. Analytical data are also in accordance with the proposed pentacyclic structure of compound **4**.

*3.2. Photophysical properties and quantum-chemical investigations of **3** and **4***

These compounds were spectrally characterized by using an UV-Vis spectrophotometer and a fluorescence spectrophotometer. The wavelength range of both spectrophotometers is 200 nm-1000 nm. The electronic absorption spectra of compounds **3** and **4** were recorded at concentration of 5×10^{-5} mol L^{-1} and their fluorescence emission spectra were obtained at concentrations of 1×10^{-6} and 5×10^{-5} mol L^{-1} in chloroform, respectively. The solvatochromic properties of compounds **3** and **4** in different solvents were also investigated (Figures 1 and 2). The absorption and emission spectra of **3** and **4** in polar solvents undergo a relatively modest red shift. Increasing the solvent polarity stabilizes the excited-state molecule relative to the ground-state molecule with the observed red shift of the absorption maximum as the experimentally observed result (Tables 1). For example, in the absorption and emission spectra of compound **3**, λ_{abs} and λ_{flu} shift from 455 to 490 nm and 485 to 540 nm respectively, as the solvent changes from cyclohexane to DMF (Table 1).

Values of extinction coefficient (ε) were calculated as the slope of the plot of absorbance *vs* concentration. The fluorescence excitation (λ_{ex}) wavelength at 380 nm (λ_{ex} /nm) was used for compounds **3** and **4**.

<Table 1>

<Figure 1>

<Figure 2>

As can be seen from Table 1, Figures 1 and 2, dye **3** showed the higher maximum absorption wavelength (λ_{abs}) at 475 nm than λ_{abs} of **4** (425 nm) in chloroform. Furthermore, in the UV-visible absorption spectrum of compound **3,** there are two absorption peaks into the visible region compared to **4** which has an absorption band in this area. To gain a deeper insight into the role of HOMO and LUMO frontier orbitals in the UV-visible absorption spectra of compounds **3** and **4**, we performed DFT calculations at the B3LYP/6-311++G(d,p) level and obtained the optimized geometries and HOMO and LUMO frontier orbitals of fluorescent dyes **3** and **4**. The optimized geometries of compounds **3** and **4** can be found in Figure 3. In the optimized geometries of the compounds **3** and **4**, all of these rings and cyano group are essentially planar and the C=C bond lengths (1.38-1.44 Ångstrom) of the aromatic rings are in the expected range (Tables S1 and S2; see Supplementary data) [24].

The energy difference between the HOMO and LUMO frontier orbitals is one of the important characteristics of molecules, which has a determining role in such cases as electric properties, electronic spectra and photochemical reactions. The HOMO and LUMO maps of **3** and **4** are shown in Figure 4. Separation energies between the HOMO and LUMO ($\Delta\varepsilon = \varepsilon_{LUMO} - \varepsilon_{HOMO}$) in dyes **3** and **4** are 2.95 and 3.25 eV (420 and 381 nm), respectively. It can be seen from Figure 4 that dye **3** has more π-system overlap in its HOMO and LUMO frontier orbitals which led to the lower separation energy between the HOMO and LUMO compared to compound **4.** In the Supporting information (Scheme S1), neutral and some charge-separated mesomeric structures of compounds **3** and **4** are presented.

The TD-DFT electronic spectra calculations on **3** show that there are two electronic transition bands: a relatively sharp peak at 349 nm (oscillator strength: 0.3425), which can be attributed to $\pi - \pi^*$ transitions (donor endocyclic nitrogen (N16) to the acceptor CN group), and a relatively broad band at 489 nm with an oscillator strength of 0.3097, which can be linked to $\pi - \pi^*$ transitions from the donor N3 to the acceptor CN group. These electronic transition bands can be compared with the experimental values of 380 and 475 nm, respectively.

Also, the TD-DFT electronic spectra calculations on **4** show a relatively sharp peak at 414 nm (oscillator strength: 0.4606), which corresponds to the experimental data (425 nm). This peak located in the visible light range can be attributed to $\pi - \pi^*$ transitions from the donor endocyclic nitrogens (N3 and N14) to the acceptor CN group. The calculated electronic absorption spectra of compounds **3** and **4** are shown in the Supporting information.

<Figure 3>

<Figure 4>

The fluorescence quantum yields (Φ_F) of compounds **3** and **4** were determined *via* comparison methods, using fluorescein as a standard sample in 0.1 M NaOH and MeOH solution [23]. The used value of the fluorescein emission quantum yield is 0.79 and the emission quantum yields of the compounds **3** and **4** are 0.69 and 0.51, respectively. The intramolecular charge transfer (ICT) states from the donor endocyclic nitrogens to the acceptor CN group can be considered as the main reason for the fluorescence intensity of green fluorescent dyes **3** and **4** [8–10]**.** Compounds **3** and **4** are structural isomers and difference in their fluorescence intensity and fluorescence quantum yield can be attributed to the energy difference between the HOMO and LUMO frontier orbitals (It was discussed by DFT calculations) and the concentration of the electron density of two fluorophores. A more detailed discussion on the electron density of **3** and **4** is examined by AIM analysis.

The Bader theory comes of ages as a very useful tool to analyze intra- and intermolecular interactions.

The main difference between the studied **3** and **4** dyes and other similar dyes, in which the structures are planar, is principally associated to the π-electronic structure. The cyano fragment, having a completely planar structure, plays an acceptor role of the photo excited electron phenomenon in these dyes [25].

The presence of the intramolecular interactions C···H differs concentration of electron density along the C-N bond in the cyano fragment in two isomers. The AIM analysis can prove that there is more fluorescence property in compound **3** compared to **4**.

The electron density map, ρ, of two isomers are shown in Figure 5. In this figure, the negative region is located throughout of two isomers and shown in red. At the first glance, the negative region is reliable evidence for the formation of resonance along the structures. With comparison of two the electron density maps of isomers, it illustrates that the negative region of dye **4** is weaker than that of dye **3**, explaining that the resonance in **3** is stronger than **4**. In other hand, the negative region which is located at the substituent CN part of **3** is more than **4** indicating that the electron withdrawing of CN at **3** is considerable.

It seem that CN as an electron withdrawing group has greater effect on resonance strength of aromatic ring in **3**, because hydrogen bonding between H30 and C21 of CN group can be affect the strength of CN electron withdrawing. Since it makes aromatic rings active, so the resonance considerably locates on the structure of **3**.

All of these data are reliable evidence for strength of the intramolecular hydrogen bond and define that formation of the dye **3** is much probable to show fluorescence effect than the dye **4**.

<Figure 5>

The parameters such as the Laplacian of the electron density$\nabla^2\rho$, the electron energy density H_C, the sum of the kinetics electron energy density (G_C) and the potential electron energy density (V_C), and as well as -G_C/V_C, $\delta(A,B)$ derive from the Bader theory and imply the interaction type and changing stability of bond after molecular rotate, intermolecular or intra-molecular interactions.

For a negative value of a Laplacian, $\nabla^2\rho < 0$ beyond doubt the interaction is completely covalent. If both $\nabla^2\rho$ and H_C be simultaneously positive ($\nabla^2\rho(r) > 0, H_c > 0$) which can be categorized as the interactions of closed electron shells, to which, in particular, most hydrogen bonds and van der Waals interactions belong. If $\nabla^2\rho$ be positive while H_C is negative, and the -G_C/V_C is smaller than 1, then the nature of interaction is considered as partly covalent [26].

The topological parameters, such as ρ_{BCP}, $\nabla^2\rho$, G_C, V_C, ($-G_C/V_C$) and H_C at the BCP (bond critical point**)** of C···H , C−N and C−C for two isomers are represented in Table 2. It appears from the molecular graphs that there are a BCP between the C···H atoms, which are connected through two bond paths. The topological structure shows that the intramolecular C···H bond

existed in the structure of molecule **3**. From the data shown in Table 2, the following results can be drawn: for the BCP of the C···H, the $\nabla^2\rho$, H are positive, and the ratio of G_C to V_C, $-G_C/V_C$, ranges up than 1; therefore, all values of topological parameters imply that the intramolecular C···H bond, is rather van der Waals in dye **3** [27–30]. From Table 2, it seems that due to hydrogen intramolecular interactions and increase in electron donating of nitrogen in pyridine ring, affected by N14 of imidazol ring, ρ_{BCP} at the BCP of C7-N10, C11-N14, N14-C15 increased. It is deserve to mention that intramolecular interactions bond could help to improve resonance by decrease efficiency of withdrawing electron CN substituent in the structures.

<**Table 2**>

The RCP (ring critical point) is a point of minimum electron density within the ring surface and a maximum on the ring line [31–33]. Table 3 gives the information about electron density ρ_{RCP} at the RCP and $\nabla^2\rho_{RCP}$ of the pyridine, imidazole and chelate ring which produced by the intra-intermolecular interaction.

<**Table 3**>

From Table 3, the value of the electron density ρ_{RCP}, $\nabla^2\rho_{RCP}$ and K reveal this fact that pyridine ring is unstable with decreasing the electron withdrawing strength of CN substituent.
On other hand, it can be seen that -C1 - C2 - N3 - C4 - C5 - C6- and -N3 - C4 - N9 - C8 - C7- ring in affected of efficiency the electron withdrawing CN substituent could be stable in **3** and the -C11 - C12 - N16 - C15 - N14-ring and -N14 - C15 - C22 - C21 - C20 - C19-ring is stable in **4**.
As mentioned before, dye **4** is much stable than dye **3**, which assures that resonance increasing in structure due to deactivation of CN substituent is the reason of this variation.

4. Conclusion

In conclusion, we have synthesized two new green fluorescent heterocyclic systems dipyrido[1',2':1,2]imidazo[4,5-*b*:4,5-*e*]pyridine-13-carbonitrile and pyrido[1',2':1,2]imidazo[4,5-*b*]pyrido[2',1':2,3]imidazo[4,5-*e*]pyridine-13-carbonitrile in excellent yields which demonstrate

interesting optical properties including high extinction coefficients and high quantum yields. DFT and TD-DFT calculations on these fluorophores were performed to gain a deeper insight into their spectroscopic properties by using the B3LYP hybrid functional and the 6-311++G(d,p) basis set. The results showed that the geometries of two dyes were rigid and planar and the separation energies between the HOMO and LUMO in dyes **3** and **4** were 2.95 and 3.25 eV, respectively. In addition, AIM analysis was conducted to investigate the QTAIM molecular graph, electron density *iso*-surface map, intra- and intermolecular interactions in these fluorophores. The results show that concentration of electron density through the C-N bond in the cyano fragment of two dyes is different, because of the intramolecular interactions $H_{(30)}\cdots C_{(CN)}$ and increase in electron donating of nitrogen in pyridine ring in fluorophore **3** which could help to improve resonance by decrease efficiency of withdrawing electron CN substituent in the structure. Comparing the quantum-chemical investigations with the experimental results reveals that they are in good agreement and DFT and TD-DFT calculations and AIM analysis can prove the higher maximum absorption wavelength and the fluorescence intensity in fluorophore **3** compared to **4**.

Acknowledgment

We would like to express our sincere gratitude to Research Office, Mashhad Branch, Islamic Azad University, Mashhad-Iran, for financial support of this work.

References

1. K.S. Gudmundsson, B.A. Johns, Org. Lett. 5 (2003) 1369.
2. Z. Wu, M.E. Fraley, M.T. Bilodeau, M.L. Kaufman, E.S. Tasber, A.E. Balitza, G.D. Hartman, K.E. Coll, K. Rickert, J. Shipmann, et al., Bioorg. Med. Chem. Lett. 14 (2004) 909.
3. A. Geronikaki, E. Babaev, J. Dearden, W. Dehaen, D. Filimonov, I. Galaeva, V. Krajneva, A. Lagunin, F. Macaev, G. Molodavkin, et al., Bioorg. Med. Chem. Lett. 12 (2004) 6559.
4. P.C. Lima, M.A. Avery, B.L. Tekwani, H. de, M. Alves, E.J. Barreiro, C.A.M. Fraga, Farmaco 57 (2002) 825.
5. G. Trapani, M. Franco, L. Ricciardi, A. Latrofa, G. Genchi, E. Sanna, F. Tuveri, E. Cagetti, G. Biggio, G. Liso, J. Med. Chem. 40 (1997) 3109.
6. M.A. Ismail, R. Brun, T. Wenzler, F.A. Tanious, W.D. Wilson, D.W. Boykin, J. Med. Chem. 47 (2004) 3658.
7. Y. Abe, H. Kayakiri, S. Satoh, T. Inoue, Y. Sawada, N. Inamura, M. Asano, C. Hatori, H. Sawai, T. Oku, et al., J. Med. Chem. 41 (1998) 4053.
8. M. Rahimizadeh, M. Pordel, M. Bakavoli, H. Eshghi, Dyes Pigm. 86 (2010)266.
9. M.M.F. Baf, M. Pordel, L.R. Daghigh, Tetrahedron Lett. 55 (2014) 6925.
10. M. Rahimizadeh, M. Pordel, M. Ranaei, M. Bakavoli, J. Heterocycl. Chem. 49 (2012) 208.
11. S. Razmara, M. Pordel, M. Ebrahimi, Chem. Hetero. Comp. 51 (2015) 713.
12. J.P. Paolini, R. K. Robins, J. Org. Chem. 30 (1965) 4085.
13. H.R. Snyder, E.L. Eliel, J. Am. Chem. Soc. 70 (1948) 1703.
14. M.D. Crozet, C. Castera, M. Kaafarani, M.P. Crozet, P. Vanelle, Arkivoc x (2003) 273.
15. , M.J. Frisch, G.W. Trucks, H. B.Schlegel, G. E. Scuseria, M.A. Robb, J.R. Cheeseman, V.G. Zakrzewski, J.A. Montgomery, R.E. Stratmann, J.C. Burant, S. Dapprich, J.M. Millam, A.D. Daniels, K.N. Kudin, M.C. Strain, O. Farkas, J. Tomasi, V. Barone, M. Cossi, R. Cammi, B. Mennucci, C. Pomelli, C. Adamo, S. Clifford, J. Ochterski, G.A. Petersson, P.Y. Ayala, Q. Cui, K. Morokuma, D.K. Malick, A.D. Rabuck, K. Raghavachari, J.B. Foresman, J. Cioslowski, J.V. Ortiz, B.B. Stefanov, G. Liu, A.

Liashenko, P. Piskorz, I. Komaromi, R. Gomperts, R.L. Martin, D.J. Fox, T. Keith, M.A. Al-Laham; C.Y. Peng, A. Nanayakkara, C. Gonzalez, M. Challacombe, P.M.W. Gill, B. G. Johnson, W. Chen, M.W. Wong, J. L. Andres, M. Head-Gordon, E.S. Replogle, J.A. Pople, Gaussian 98, Revision A.7; Gaussian, Inc.: Pittsburgh PA, 1998.

16. C. Lee, W. Yang, R.G. Parr, Phys. Rev. B 37 (1988) 785.
17. J. Tomasi, R. Cammi, J. Comput. Chem. 16 (1995) 1449.
18. E. Runge, E.K.U. Gross, Phys. Rev. Lett. 52 (1984) 997.
19. M. Petersilka, U.J. Gossmann, E.K.U. Gross, Phys. Rev. Lett. 76 (1966) 1212.
20. R. Bauernschmitt, R. Ahlrichs, Chem. Phys. Lett. 256 (1996) 454.
21. M. MaKosza, K. Wojciechowski, Chem. Rev. 104 (2004) 2631.
22. R. Sahraei, M. Pordel, H. Behmadi, B. Razavi, J. Lumin. 136 (2013) 334.
23. J.Q. Umberger, V.K. LaMer, J. Am. Chem. Soc. 67 (1945) 1099.
24. H. Dal, Y. Süzen, E. Sahin, Spectrochim. Acta Part A 67 (2007) 808.
25. V. Maroofi, M. Pordel, H. Chegini, Sh. Ramezani, J. Fluoresc. 25 (2015) 1235.
26. M. Vener, A. Manaev, A. Egorova, V. Tsirelson, J. Phys. Chem. A, 111 (2007) 1155.
27. I. Mata, I. Alkorta, E. Molins, E. Espinosa, Chem.-Eur. J. 16 (2010) 2442.
28. T.M. Krygowski, J.E. Zachara-Horeglad, M. Palusiak, S. Pelloni, P. Lazzeretti, J. Org. Chem. 73 (2008) 2138.
29. X. Li, Y. Wang, S. Zheng, L. Meng, Struct. Chem. 23 (2012) 1233.
30. R.F. Bader, M.T. Carroll, J.R. Cheeseman, C. Chang, J. Am. Chem. Soc. 109 (1987) 7968.
31. H. Eshtiagh-Hosseini, S. Ali Beyramabadi, A. Morsali, M. Mirzaei, H. Chegini, M. Elahi, M.A. Naseri, J. Mol.Struc. (2014).
32. S. Mitra, A.K. Chandra, P.M. Gashnga, S. Jenkins, S.R. Kirk, J. Mol. Model. 18 (2012) 4225.
33. H. Chegini, S.A. Beyramabadi, A. Morsali, M. Saberi, M. Lotfi, J.Mo. Struc. 1083 (2015) 1.

Schemes

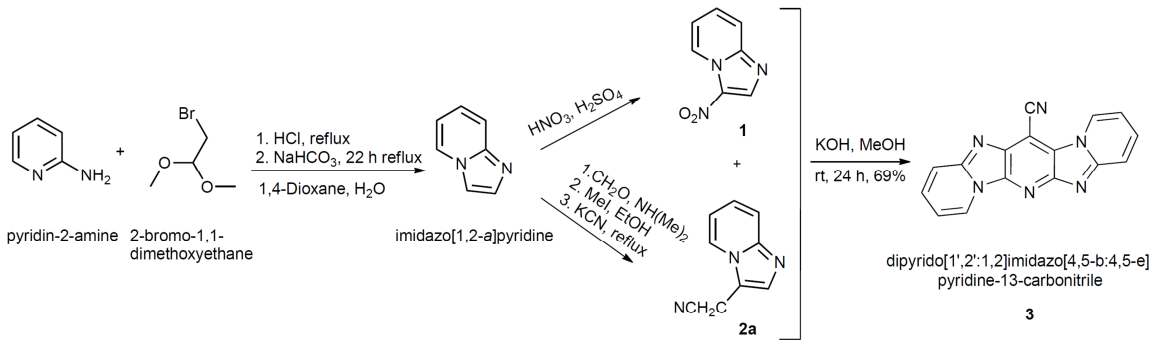

Scheme 1. Synthesis of new fluorescent dye **3.**

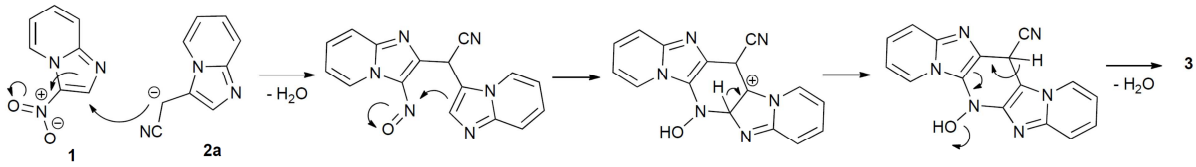

Scheme 2. The proposed reaction mechanism for the formation of **3.**

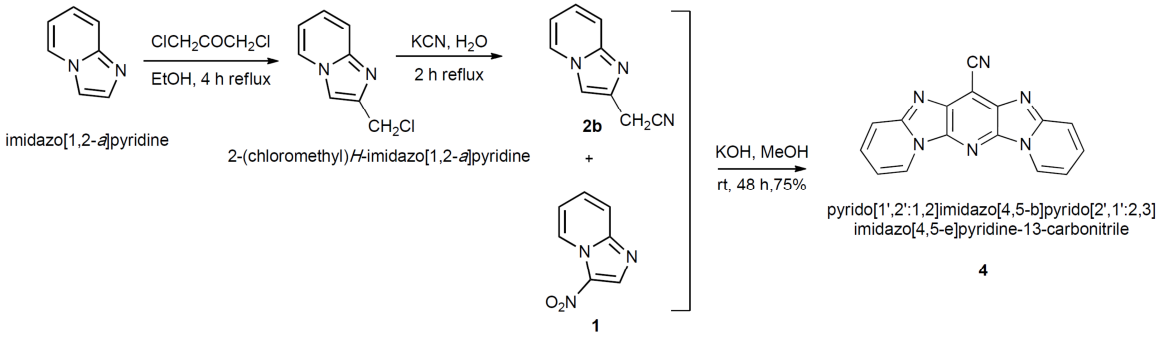

Scheme 3. Synthesis of new fluorescent dye **4.**

Figures

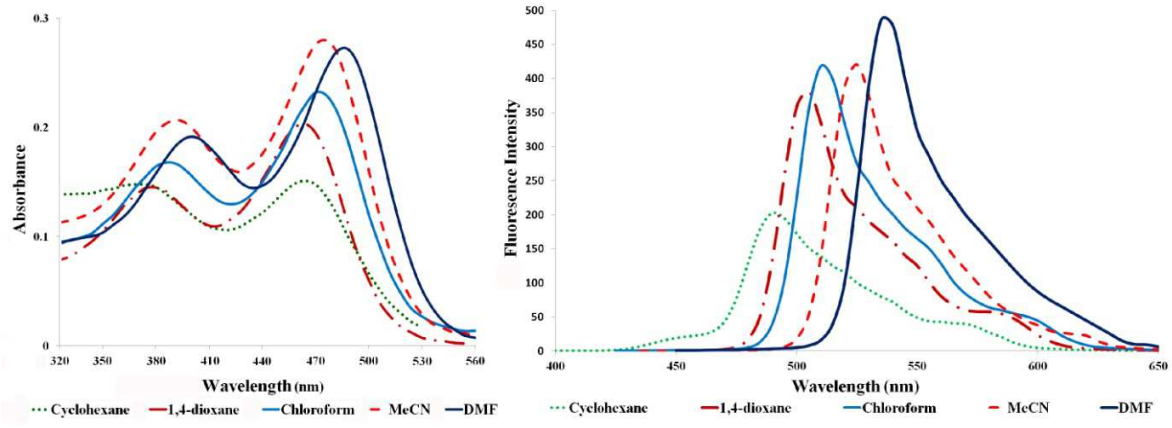

Figure 1. Visible absorption (left) (5×10^{-5} mol L^{-1}) and emission spectra (right) (1×10^{-6} mol L^{-1}) of compound **3** in different solvents.

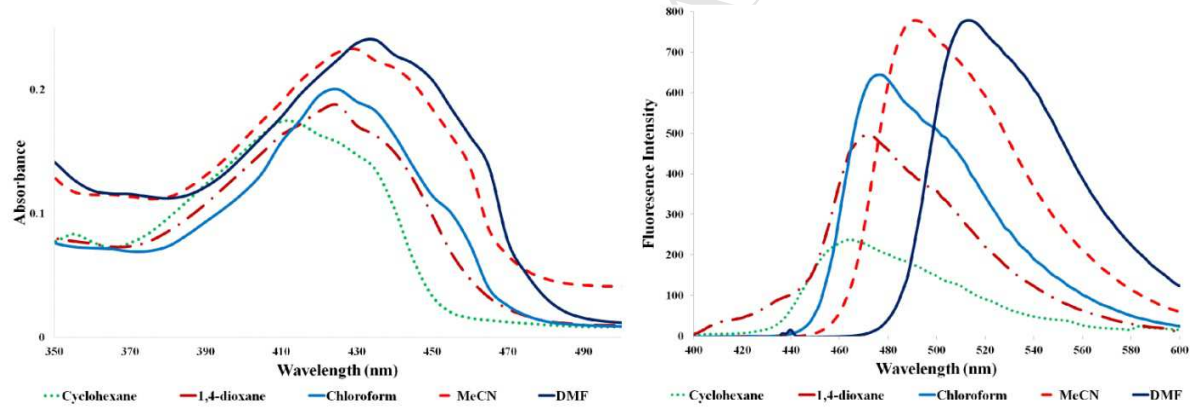

Figure 2. Visible absorption (left) (5×10^{-5} mol L^{-1}) and emission spectra (right) (5×10^{-5} mol L^{-1}) of compound **4** in different solvents.

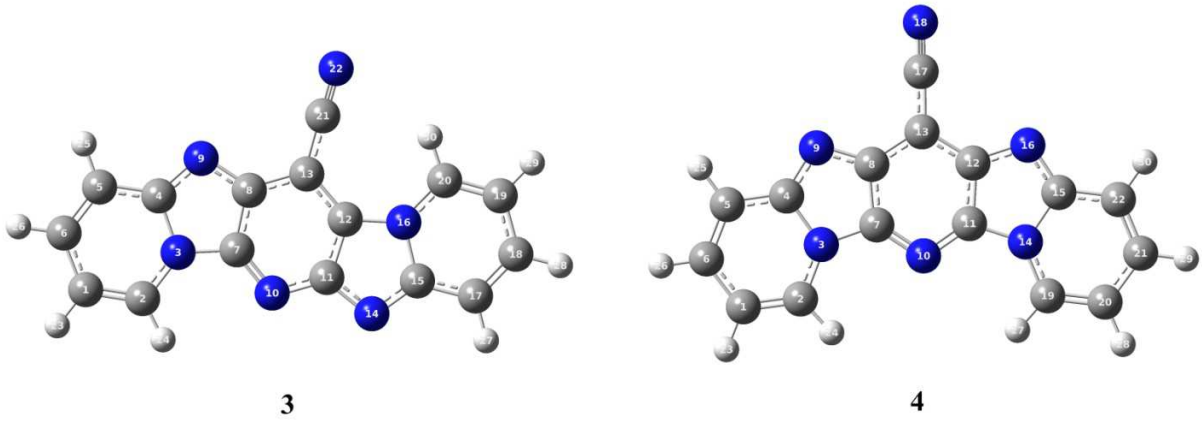

3 4

Figure 3. Optimized geometries of the compounds **3** and **4**

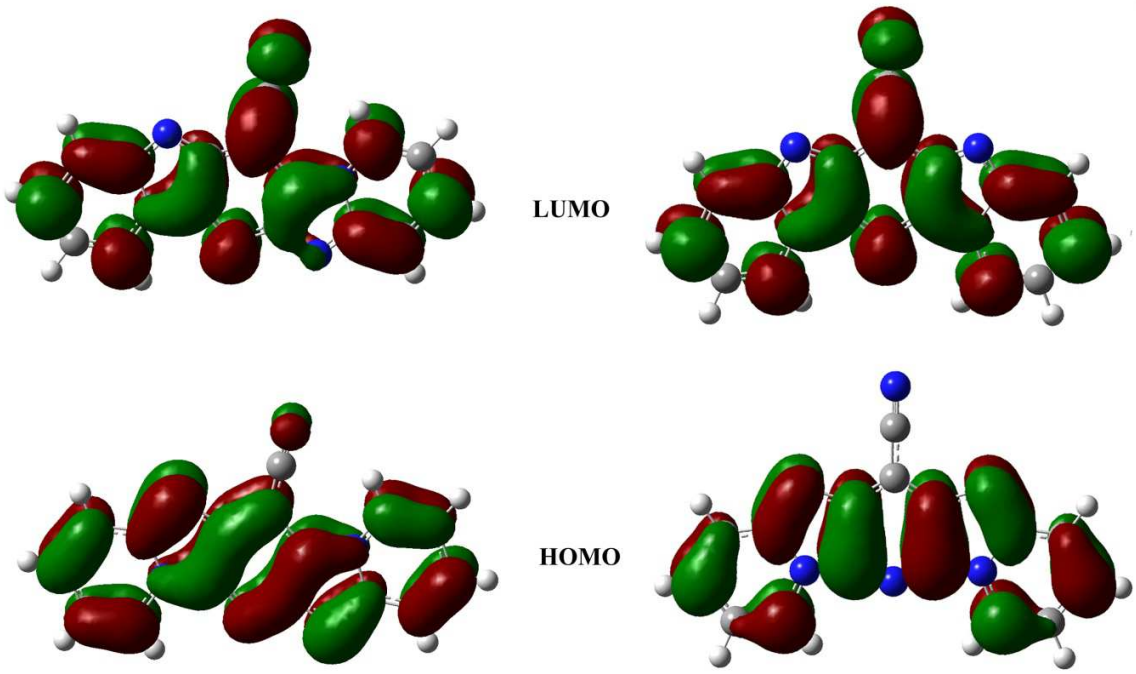

Figure 4. The HOMO and LUMO frontier orbitals of the compounds **3** (left) and **4** (right).

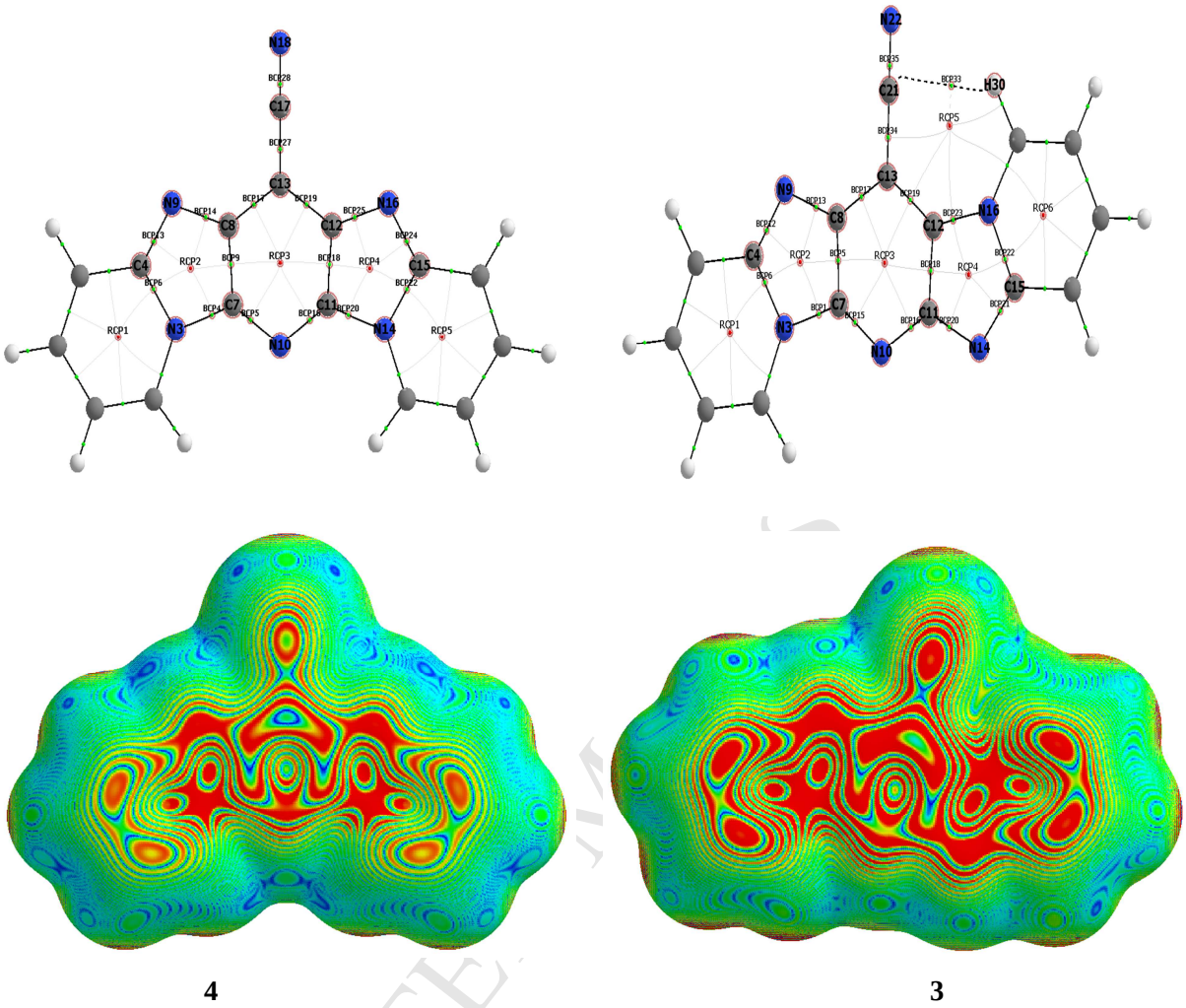

Figure 5. The QTAIM molecular graph and electron density iso-surface map of two isomers.

Tables

Table 1. Spectroscopic data for green fluorescent dyes **3** and **4** at 298 K in different solvents.

Solvent	**3** λ_{abs} (nm)[a]	**4** λ_{abs} (nm)	**3** $\varepsilon \times 10^{-4}$ [(mol L^{-1})$^{-1}$ cm^{-1}][b]	**4** $\varepsilon \times 10^{-4}$ [(mol L^{-1})$^{-1}$ cm^{-1}]	**3** λ_{ex} (nm)[c]	**4** λ_{ex} (nm)	**3** λ_{flu} (nm)[d]	**4** λ_{flu} (nm)
DMF	490, 400	435	5.2	5.0	490	435	540	515
CH_3CN	480,385	430	5.4	4.8	480	430	525	495
Chloroform	475,380	425	4.6	3.6	475	425	510	475
1,4-Dioxane	460,375	425	3.6	3.2	460	425	505	470
Cyclohexane	455,370	410	2.6	2.5	455	410	485	460

[a] Wavelengths of maximum absorbance (λ_{abs}); [b] Extinction coefficient; [c] Wavelengths of fluorescence excitation (λ_{ex}); [d] Wavelengths of fluorescence emission (λ_{flu}).

Table2: The topological properties at the BCP for two isomers.

$Atoms$	BPL	$\|q(A,B)\|$	$\delta(A,B)$	ρ	$\nabla^2\rho$	G	V	H	$-G/V$
				3					
C11 - C12	2.7139	0.0200	1.0962	0.293628	-0.76866	0.089275	-0.37071	-0.28144	0.240819
C11 - N14	2.5782	0.4517	1.1620	0.329337	-0.98884	0.176797	-0.6008	-0.42401	0.294268
C12 - C13	2.6488	0.0767	1.2835	0.300357	-0.80403	0.098383	-0.39777	-0.29939	0.247334
C12 - N16	2.6176	0.2831	1.0359	0.296774	-0.71618	0.225097	-0.62924	-0.40414	0.357729
C13 - C21	2.6872	0.2438	1.1021	0.281924	-0.77272	0.086125	-0.36543	-0.2793	0.235683
C15 - N16	2.6763	0.3628	0.9585	0.284414	-0.74123	0.180386	-0.54608	-0.36569	0.33033
C21 - N22	2.1854	1.1313	2.3450	0.477002	-0.31516	0.779748	-1.63829	-0.85854	0.475953
C4 - N9	2.5209	0.6388	1.2916	0.352293	-1.08969	0.205309	-0.68304	-0.47773	0.300582
C7 - C8	2.7024	0.0419	1.0935	0.297812	-0.79642	0.09031	-0.37973	-0.28942	0.23783
C7 - N10	2.4861	0.6165	1.2967	0.357278	-1.04229	0.257817	-0.77621	-0.51839	0.332149
C8 - C13	2.6647	0.0758	1.2278	0.299025	-0.81115	0.09278	-0.38835	-0.29557	0.238909
C8 - N9	2.5744	0.4285	1.2190	0.328508	-0.97089	0.179208	-0.60114	-0.42193	0.298114
N10 - C11	2.5358	0.5112	1.1914	0.336696	-0.98265	0.229049	-0.70376	-0.47471	0.325465
N14 - C15	2.5053	0.6309	1.3116	0.358186	-1.1129	0.219063	-0.71635	-0.49729	0.305804
N3 - C4	2.6573	0.3639	0.9703	0.290396	-0.75896	0.193058	-0.57585	-0.3828	0.335255
N3 - C7	2.6315	0.2614	0.9634	0.295408	-0.75201	0.209221	-0.60645	-0.39723	0.344995
C21 - H30	5.1053	0.0199	0.0192	0.008844	0.029026	0.005884	-0.00451	0.001373	1.304367
				4					
C11 - C12	2.7030	0.0609	1.0996	0.297427	-0.79346	0.090518	-0.3794	-0.28889	0.23858
C11 - N14	2.6267	0.2730	0.9710	0.296368	-0.74393	0.214891	-0.61576	-0.40087	0.348983
C12 - C13	2.6652	0.0963	1.2388	0.299182	-0.81094	0.092454	-0.38764	-0.29519	0.238504
C12 - N16	2.5765	0.4239	1.2159	0.327987	-0.972	0.177973	-0.59895	-0.42097	0.297144
C13 - C17	2.6845	0.2660	1.1050	0.282855	-0.7776	0.086425	-0.36725	-0.28082	0.235331
C15 - N16	2.5202	0.6417	1.2942	0.352931	-1.09361	0.204648	-0.6827	-0.47805	0.299763
C17 - N18	2.1853	1.1451	2.3500	0.47703	-0.31816	0.778999	-1.63754	-0.85854	0.475714
C4 - N9	2.5202	0.6415	1.2944	0.352931	-1.09361	0.204648	-0.6827	-0.47805	0.299764
C7 - C8	2.7030	0.0608	1.0995	0.297427	-0.79346	0.090518	-0.3794	-0.28888	0.238581
C7 - N10	2.5005	0.5698	1.2604	0.348816	-0.98546	0.25785	-0.76207	-0.50422	0.338357
C8 - C13	2.6652	0.0963	1.2388	0.299181	-0.81094	0.092454	-0.38764	-0.29519	0.238504
C8 - N9	2.5765	0.4241	1.2158	0.327987	-0.972	0.177973	-0.59895	-0.42097	0.297144
N10 - C11	2.5005	0.5700	1.2603	0.348816	-0.98546	0.257849	-0.76206	-0.50421	0.338357
N14 - C15	2.6586	0.3598	0.9694	0.289609	-0.75228	0.193787	-0.57564	-0.38186	0.336644
N3 - C4	2.6586	0.3597	0.9695	0.289609	-0.75228	0.193789	-0.57565	-0.38186	0.336645
N3 - C7	2.6267	0.2733	0.9710	0.296368	-0.74393	0.214889	-0.61576	-0.40087	0.348981

Table 3. The topological properties at the RCP for two isomers.

	Atoms	ρ	$\nabla^2 \rho$	K
3	-C1 - C2 - N3 - C4 - C5 - C6-	0.021377	0.158132	-0.007667
	-N3 - C4 - N9 - C8 - C7-	0.052564	0.369192	-0.006408
	-C7 - C8 - C13 - C12 - C11 - N10-	0.023285	0.161113	-0.006892
	-C11 - C12 - N16 - C15 - N14-	0.052430	0.367555	-0.006482
	-C12 - C13 - C21 - H30 - C20 - N16-	0.006912	0.033775	-0.001962
	-C15 - N16 - C20 - C19 - C18 - C17-	0.021062	0.155754	-0.007581
4	-C1 - C2 - N3 - C4 - C5 - C6-	0.021361	0.158005	-0.007660
	-N3 - C4 - N9 - C8 - C7-	0.052520	0.368736	-0.006428
	-C7 - C8 - C13 - C12 - C11 - N10-	0.023456	0.162075	-0.006862
	-C11 - C12 - N16 - C15 - N14-	0.052520	0.368736	-0.006428
	-N14 - C15 - C22 - C21 - C20 - C19-	0.021361	0.158005	-0.007660

Highlights

- Two new fluorescent heterocyclic systems were synthesized from imidazo[1,2-*a*]pyridine.
- The optical and solvatochromic properties of these fluorophores were investigated.
- DFT calculations of two structures are performed at the B3LYP/6-311++G(d,p) level.
- Their intra- and intermolecular interactions were investigated by AIM analysis.